I. SUPPLEMENTARY INFORMATION FOR "CHARACTERIZATION OF HEAT TRANSFER IN 3D CMOS STRUCTURES USING SIDEBAND SCANNING THERMAL WAVE MICROSCOPY"

SUPPORTING INFORMATION

A. Experimental details

This work was realised on a modified Thorlabs Atomic Force Microscope (Thorlabs Inc). The probe used consists of a triangular shaped silicon nitride probe with a microfabricated Pd element at its apex. This thermometer is then connected by two evaporated gold lines and pads.[1] (K-TEK Nanotechnology) The excitation and demodulation of the AC signals were performed on a HF2LI lock-in amplifier (Zürich instruments). The demodulation of the resulting sideband modulation was done directly using an amplitude/frequency modulation add-on implemented on the lock-in amplifier, assuring the syncing of the oscillators.

B. Diode IV characteristic and thermal response

In the case of a diode under a unipolar excitation, only the part of the voltage signal that reaches the switching voltage produces an effective heating. This is demonstrated at Figure 1 where the sideband demodulated amplitude is plotted against the DC offset of the sine wave for different driving peak-to-peak amplitudes. For a twice greater driving amplitude, the switching point of the diode will be reached for an offset that is lower by half the peak-to-peak amplitude which is verified here. In addition, the curves reproduce the exponential switching of the diode under study followed by a linear increased in the forward passing regime. The switching voltage obtained is around 2.3 V. This is in-line with IV characteristic of the diode, see Figure 2 and this confirms the importance of considering the non-linearity of the heater in this study.

C. Sideband detection of self-heating in a pure resistance driven with unipolar signal

This section will provide a simplified picture, useful to understand the sideband detection of thermal wave that has been introduced in this work. This section assumes a pure resistive be-

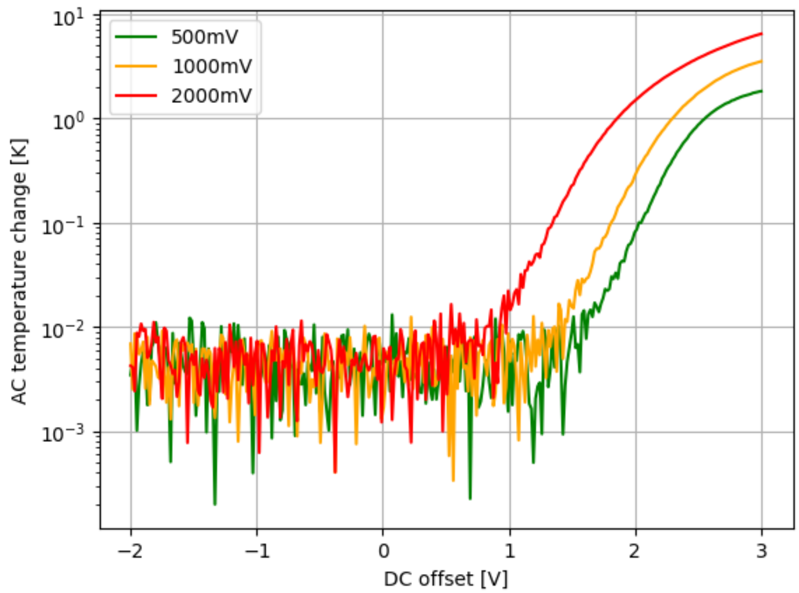

FIG. 1. Temperature change on the surface extracted from the first demodulated sideband with respect to the DC offset applied on the diode driving signal. The different colours indicate different driving amplitudes.

haviour for the heater to simplify the equations. The proper signal treatment, considering a non-uniform power spectrum arising from the diode, is provided in the main text.

If one assumes that the heater behaves as a simple resistance, the Joule heating generated can be written as :

$$Q = \frac{V_{\text{mod}}^2}{2R} \tag{1}$$

where Q is the total heat generated on the whole element, V is the voltage signal applied on it and R is its resistance. For an unipolar sine wave driving signal, at an angular frequency ω_m :

$$V_{\text{mod}}(t) = V_{mod,0}\big(1 + \sin(\omega_1 t + \phi)\big) \tag{2}$$

where $V_{mod,0}$ is the amplitude of the signal and ϕ an arbitrary phase. For the following development, one assumes that the phase of the probe's reading signal is set to 0 while the other signal are phased compared to it. Thus the temperature variation on the surface generated by the diode can be written as :

$$\Delta T_s(t,x,y) = \gamma(x,y)\frac{V_{mod,0}^2}{2R}\big[\frac{3}{2} + 2\sin(\omega_1 t + \phi - \omega_1 t_p) \tag{3}$$

$$-\frac{1}{2}\sin(2\omega_1 t + 2\phi - 2\omega_1 t_p)\big] \tag{4}$$

$$\tag{5}$$

where γ is a factor that links the heat generated by the diode below the surface to an actual temperature change at the interface with the probes, it contains the geometrical spreading of the heat, the interfaces etc. t_p is the propagation time of the heat wave from the self-heating diode to the probe, thus the angular frequency of the heat wave multiplied by this time gives the phase lag accumulated by the heat wave. As can be seen, the unipolar excitation of the diode (treated as a resistance R) gives rise to a temperature signal in DC, first and second harmonic frequency windows.

Once the wave has reached the probe, the temperature variation on the surface modulates the amplitude of the SThM signal read by the thermometer. This can be understood as an amplitude modulation of the voltage across the Wheatstone bridge which is ultimately the signal measured. The intermixing with the probe's high frequency driving signal arises. This intermixing produces the sidebands that are used for detection.

$$V_{\mathrm{car}} = V_{car,0}\sin(\omega_c t) \tag{6}$$

$$V_{\mathrm{car}}^{AM} = V_{\mathrm{car}}\Delta T_s \xi \tag{7}$$

The resulting amplitude modulated signal V_{car}^{AM} can be written as follows:

$$\begin{aligned} V_{\mathrm{car}}^{AM} = \xi\gamma\frac{V_{mod,0}^2 V_{car,0}}{2R}\Big[&\sin(\omega_c t) \\ &+\cos\big((\omega_c-\omega_{1f})t-\phi-\omega_{1f}t_p\big) \\ &-\cos\big((\omega_c+\omega_{1f})t+\phi+\omega_{1f}t_p\big) \\ &-\frac{1}{4}\sin\big((\omega_c-\omega_{2f})t-2\phi-\omega_{2f}t_p\big) \\ &-\frac{1}{4}\sin\big((\omega_c+\omega_{2f})t+2\phi+\omega_{2f}t_p\big)\Big] \end{aligned} \tag{8}$$

ξ is the sensitivity of the SThM probe, expressed as the expected change of voltage of the thermometer element for a 1 K temperature change on the surface. γ is the temperature change on the surface for one volt applied on the heating diode. ω_c, ω_{1f} and ω_{2f} are respectively the angular frequencies of the carrier signal, of the first and second harmonics of the diode's excitation. V_{car} and V_{mod} are respectively the amplitudes of the voltage used for the reading of the Wheatstone bridge, *i.e.* the carrier signal, and the modulation of its amplitude created by the oscillating temperature on the surface. ϕ is an arbitrary phase lag between the oscillator responsible for the probe reading and the oscillator sourcing the diode's excitation voltage. t_p is the propagation time from the heating element to the SThM probe, which depends the distance between them, the material properties as well as its interfaces.

The first harmonic and second harmonic terms each yield their own sub-bands while the DC component gives a component at the carrier frequency, which will appear in the SThM signal at 91kHz. We can also see that, for an unipolar driving signal, the second harmonic generation is expected to be a fourth of the sub-band signal when considering a perfect resistor. This is qualitatively verified when one sweeps the dc offset on the signal, on Figure 1

D. Details about the sample

The surface regions above the metallic islands (and the pad edges) have an elevated height, approximately 3 µm increased from the inter-island regions, consistent with the 2.8 µm Al top metal thickness noted for chip-package interaction (CPI) qualification of the 22FDX process[2]. Between the top Al and the DTSCR at the FEOL, a metal stack consistent with one of the CPI-qualified BEOL options for 22FDX[2] is used: 7 layers of thin metal with low-K/ultra-low-K (ULK) dielectric, 1 layer of thick metal with TEOS (tetraethyl orthosilicate) dielectric, and 1 layer of ultra-thick metal (UTM) with TEOS dielectric. Specification of TEOS typically corresponds to its use in manufacturing as a precursor for an oxide such as SiO_2 which would then act as the inter-metal dielectric for those layers[3]. Each of these buried metal layers is Cu, and the height of the top of the UTM layer relative to the active device layer (e.g. the DTSCR) is ~ 6.9 µm as given for 22FDX metal stack #11[4]. Each of these metal layers has a similar fill of smaller floating metallic islands along with some signal routing lines, but the presence of inter-metal dielectric means that these metal patterns do not have a significant effect on the chip's physical surface topography. Beneath the diode, the backplane silicon substrate of the chip is 254 µm thick and mounted to a PCB using a silver adhesive.

The DTSCR power dissipation is distributed non-uniformly over a significant area. The junction area of the three diodes in Figure 2a are given as $A_{D1} = 21.12\,\mu m^2$ and $A_{D2} = A_{D3} = 3.52\,\mu m^2$. While the junction area of diode D1 is greater than the other two, similar power levels are dissipated in each of the three diodes due to the same current passing through all three diodes and only a minor difference in forward-bias voltage resulting from the larger area of D1. These three junction areas are each distributed across multiple parallel "finger" devices laid out across a $\sim 250\,\mu m^2$ region denoted via the blue rectangle in the micrograph presented in Figure 3a.

E. Amplitude-dependent sideband-SThM line scans

At Figure S2, different SThM traces have been recorded while increasing the diode's driving voltage amplitude. As can be seen, the amplitude of both the first and second harmonic sideband are progressively increased while the phase does not depend on this amplitude. As the phase signal reflects the propagating time of the thermal waves, this was expected and acts as the confirmation of the relevance of our thermal wave analysis, provided in the main text.

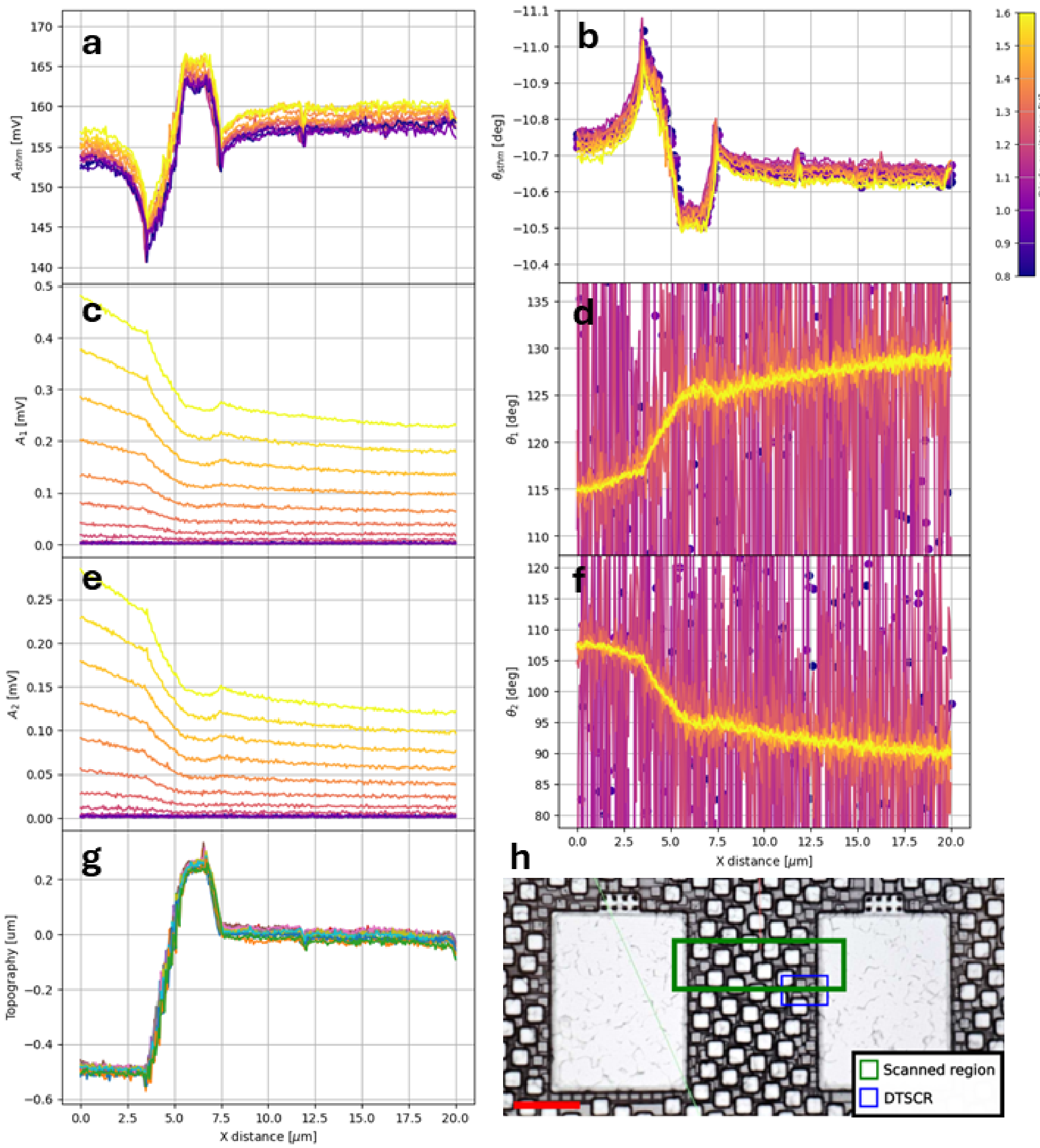

FIG. 2. Power-dependent study on the buried diode. The color scale presented on the top right denotes the amplitude of the voltage excitation applied on the diode. **a** and **b** are respectively the amplitude and phase of the signal at 91kHz. **c** and **d** are respectively the amplitude and phase traces of the first harmonic sideband at 92kHz. **e** and **f** are respectively the amplitude and phase traces of the second harmonic sideband at 93kHz. **g** is topography traces obtained for the different powers. **h** presented the micrograph of the region of interest, the dashed line indicates where the traces were recorded. The shaded red region is the place where the heating diode is buried as identified by the maps presented at Figure 2 of the main article.

REFERENCES

[1]P. S. Dobson, J. M. R. Weaver, and G. Mills, “New Methods for Calibrated Scanning Thermal Microscopy (SThM),” in *2007 IEEE SENSORS*, Oct. 2007, pp. 708–711. [Online]. Available: https://ieeexplore.ieee.org/abstract/document/4388498

[2]C. Klewer, F. Kuechenmeister, J. Paul, D. Breuer, B. Boehme, J. K. Cho, S. Capecchi, and M. Thiele, “Package Qualification Envelope for 22fdx® Technology,” *IMAPSource Proceedings*, vol. 2019, no. 1, pp. 169–175, oct 1 2019.

[3]D. Bulla and N. Morimoto, “Deposition of thick teos pecvd silicon oxide layers for integrated optical waveguide applications,” *Thin Solid Films*, vol. 334, no. 1, pp. 60–64, 1998. [Online]. Available: https://www.sciencedirect.com/science/article/pii/S0040609098011171

[4]N. Wu, “22fdsoi technology for fully-integrated mmw and radar applications,” in *2020 23rd International Microwave and Radar Conference (MIKON)*, 2020.